Relationships among Forearc Structure, Fault Slip, and Earthquake Magnitude: Numerical Simulations with Applications to the Central Chilean Margin

Xiaoyu Wang[1,1], Julia Morgan[2,2], and Nathan Bangs[3,3]

[1]Rice University
[2]Department of Earth Science, Rice University, Houston, Texas, USA
[3]University of Texas, Institute for Geophysics, Austin, TX

December 1, 2022

Abstract

Two adjacent segments of the Chile margin exhibit significant differences in earthquake magnitude and rupture extents during the 1960 Valdivia and 2010 Maule earthquakes. We use the Discrete Element Method to simulate the upper plate as having an inner and outer wedge defined by different frictional domains along the decollement. We find that outer wedge width strongly influences coseismic slip distributions. We use the published peak slip magnitudes to pick best fit slip distributions and compare our models to geophysical constraints on outer wedge widths for the margins. We obtain reasonable fits to published slip distributions for the 2010 Maule rupture. Our best-fit slip distribution for the 1960 Valdivia earthquake suggests that peak slip occurred close to the trench, differing from published models but being supported by new seismic interpretations along this margin. Finally, we also demonstrate that frictional conditions beneath the outer wedge can affect the coseismic slip distributions.

Journal of Geophysical Research

Supporting Information for

Relationships among Forearc Structure, Fault Slip, and Earthquake Magnitude: Numerical Simulations with Applications to the Central Chilean Margin

Xiaoyu Wang[1], Julia K. Morgan[1], Nathan Bangs[2]

[1] Department of Earth, Environmental and Planetary Sciences, Rice University, Houston, Texas, USA.

[2] Institute for Geophysics, University of Texas at Austin, Austin, USA

Introduction

This supporting material introduces the basics of the discrete element method (DEM), as well as the experimental model setup, simulation workflow, and calculation of cumulative changes in stress. Moreover,

we tabulate the important mechanical and numerical parameters used to build the initial models. Finally, we tabulate the published parameters that we used to constrain/calibrate our models for 1960 Valdivia and 2010 Maule rupture segments.

Text S1. DEM Modeling

In our implementation of the discrete-element-method (DEM), we simulate an assemblage of discrete spherical particles that interact with each other according to elastic-frictional (Hertz-Mindlin) contact law. We introduce cohesion by adding a mechanical bond at interparticle contacts (Morgan, 2015). This property can allow us to simulate cohesive materials as may occur within the deeper accretionary prism. The more frontal region of a prism is approximated as non-cohesive, i.e., lacking interparticle bonds. The combination of pre-assigned interparticle contact parameters, in combination with the mechanical properties of the particles themselves, define the overall behavior of the particle assemblage. This study uses a version of DEM implemented in RICEBAL. Details about the method are provided in Morgan and Boettcher (1999), Guo and Morgan (2004; 2006), and Morgan (2015). Continuum approximations of the bulk properties and behavior of the numerical model are derived using the contact force distribution and displacement gradients. By averaging continuum properties over finite volumes, stress and strain fields can be calculated for the domain (Thornton and Barnes, 1986; Morgan and Boettcher, 1999; Morgan and McGovern, 2005b; a; Morgan, 2015).

Figure S1 shows the general model setup. The initial length of the simulated wedge is set to 200 km, comparable to the dimensions of the rupture areas in Chile Margin (Moreno *et al.* , 2010; Contreras-Reyes *et al.* , 2017). To best balance model run time and model resolution, the upper wedge is constructed of approximately 200,000 discrete particles with radii of 100, 120, 160 and 200 m. Particles are randomly generated within a two-dimensional box (400×60 km) and allowed to settle under gravity.

The mechanical properties of the simulated system are defined by the assigned particle properties and interparticle friction coefficients (Table S3). Particles within the wedge, indicated by the black and blue layers in Figure S1, are free to translate, rotate and interact as the wedge evolves. The gray particles defining the basal sliding surface are fixed in space, their small radii (10 m) ensure a relatively smooth sliding surface, unimpeded by particle roughness.

The coefficients of internal and basal sliding friction are determined by the interparticle friction coefficients assigned between wedge particles ($\mu_{\text{int}}^{\text{part}}$) and wedge and basal particles ($\mu_{\text{bas}}^{\text{part}}$) respectively. The calibrated relationships between the interparticle and bulk friction coefficients are presented in a previous study (Wang and Morgan, 2019). The assigned internal friction coefficient within the outer wedge and basal friction coefficient beneath are further annotated as$\mu_{int_outer}^{\text{part}}$ and$\mu_{bas_outer}^{\text{part}}$, respectively. Similarly, the internal and basal friction coefficients for the inner wedge are written as $\mu_{int\_inner}^{\text{part}}$ and$\mu_{bas_inner}^{\text{part}}$. We tested multiple combinations of internal and basal friction values to obtain first order fits to observed earthquake displacements along the Chile margin, and selected the following interparticle friction coefficient as initial friction conditions for our simulations: $\mu_{int\_outer}^{\text{part}} = \mu_{int\_inner}^{\text{part}} = 0.100$ (friction coefficients between wedge particles), which remains fixed throughout the simulation; initial $\mu_{bas\_outer}^{\text{part}} = \mu_{bas\_inner}^{\text{part}} = 0.040$ (friction coefficients between wedge and basal particles), which is comparable to the effective basal friction coefficient used by Wang and He (2008). Basal friction coefficients are subsequently varied during the simulations as described below and in the text.

Text S2. Simulation Workflow

We seek to simulate the dynamic Coulomb Wedge model earthquake cycle (Wang and Hu, 2006) in our simulations. We first prepare the fault for dynamic slip by preconditioning it during steady backwall displacement, holding the initial basal friction at 0.04. This represents the interseismic stage. This preconditioning ensures

high shear stress along the fault and the accumulation of elastic strain energy within the wedge. To simulate the dynamic stage of the earthquake cycle, we reduce the friction coefficient along the basal decollement beneath the inner wedge to approximate velocity weakening and either increase or maintain the basal friction beneath the outer wedge to approximate velocity strengthening.

Pre-earthquake Loading Stage

To simulate the interseismic (preconditioning) period, the right wall of the wedge moves inward at a constant horizontal velocity (v_x) of 1 m/s, under constant basal friction conditions. During this preconditioning stage, the system state is recorded at increments of 200 m of backwall displacement. The internal stresses within the wedge are supported by elastic deformation at interparticle contacts, defining the potential energy of the system. During this stage, the wedge deforms, either extending or contracting, depending on the basal friction conditions and the predefined wedge geometry. The preconditioning stage is complete when the model reaches its steady state, State 1. Details about the implementation of preconditioning and the discussion about the steady state can be found in Wang and Morgan (2019).

Once the wedge reaches State 1, we simulate the second stage of dynamic earthquake unloading, culminating in the final State 2. At the start of the second stage, the backwall displacement is stopped. Earthquake unloading is initiated by the reduction in basal friction beneath the inner wedge, and concurrent increase in friction beneath the outer wedge as appropriate.

Text S3. Mean Stress and Stress Transfer

As an indicator of elastic strain energy storage and release, we calculate gridded mean stresses (σ_m) throughout the system at different stages (Morgan, 2015; Wang and Morgan, 2019) of the simulation. The stress transfer and the corresponding energy release during earthquake unloading is approximated by plotting the cumulative change in σ_m between State 2 and State 1 of the simulation (Figure S3). A reduction (negative in blue) in σ_m indicates the release of elastic strain energy, whereas an increase (positive in red) indicates an increase in energy. No change in stress is indicated by white.

To demonstrate the role of the frictionally stronger outer wedges in modulating fault slip, we plot corresponding model-derived stress changes that accompanied the simulated earthquakes (Figure S3) for each selected models (Figure 3). In all cases, the earthquake causes a reduction in inner wedge stress, some of which is transferred toward the toe, resulting in an increase in stress within the outer wedge.

For the Maule rupture segment, the simulated coseismic stress change (Figure S3a) shows that unloading of the inner wedge transferred significant stress into the outer wedge, around 80 km, near the boundary with the inner wedge, whereas the toe of the wedge experienced essentially no change in stress. This demonstrates that the outer wedge resisted megathrust slip, limiting rupture propagation to the trench, which is consistent with expected velocity-strengthening behavior and observations (Contreras-Reyes et al., 2010; Delouis et al., 2010; Moreno et al., 2010; Maksymowicz et al., 2017).

For the simulated coseismic stress change for the Valdivia rupture segment (Figure 3b), the wedge experienced primarily coseismic stress drop, except very near the toe of the wedge, where a stress rise is observed above the strong outer wedge fault. However, despite the outer wedge resistance, our simulations suggest that the toe experienced more than 30 m of slip (Figure 3b).

Table S1. Comparison between the Maule and Valdivia Rupture Segments.

	Valdivia Rupture Area	Maule Rupture Area	Source
Earthquake Magnitude	9.5	8.8	
Strike Rupture distance	˜960 km	˜600 km	Moreno *et al.*, 2009; Moreno *et al.*, 2010 Moreno *et al.*, 2012
Peak Slip	˜44 m	˜20 m	Moreno *et al.*, 2009 Moreno *et al.*, 2010 Moreno *et al.*, 2012 Tong *et al.*, 2010
Distance of Peak Slip to the Trench	˜80 to 100 km	˜80 to 100 km	Moreno *et al.*, 2009 Moreno *et al.*, 2010 Moreno *et al.*, 2012
Outer Wedge Dimension	< 30˜40 km	>20-60km	Contreras-Reyes *et al.*, 2010, 2017 Bangs *et al.*, 2020

Table S2. Basal Friction Conditions before and after Earthquake Unloading.

Experiments	Outer Wedge Before Earthquake	Outer Wedge After Earthquake
Setup 1 Ratios of outer-wedge dimension to full wedge length: 0% - 60%	$\mu^{\text{part}}_{bas\_outer} = 0.040$	$\mu^{\text{part}}_{bas\_outer} = 0.040$
Setup 2 Ratios of outer-wedge dimension to full wedge length: 16% - 53%	$\mu^{\text{part}}_{bas\_outer} = 0.040$	$\mu^{\text{part}}_{bas\_outer} = 0.040 \mu^{\text{part}}_{bas\_out}$

Table S3. Model Parameters Used in the Simulation.

Dimensions of 2D Box Domain	400 km x 60 km
Young's Modulus for Particle (E_{particle})	2.9 E09 Pa
Particle Radii (r)	100, 120, 160, 200 m
Poisson's Ratio for Particle (v_{particle})	0.2
Density for Particle (ρ_{particle})	2500 kg/m^3
Young's (Normal) Modulus for Bond (E_{bond})	2E08 Pa
Shear Modulus for Bond (G_{bond})	2E08 Pa
Tensile strength for Bond (T_{0_bond})	4E07 Pa
Shear Strength for Bond (S_{0_bond})	8E08 Pa
Time Step/Cycle	0.05 sec/cycle
Number of Cycles/ Increment	4000 in preconditioning stage;
Rate of Backwall Displacement	1 m/s in preconditioning stage; 0 m/s in dynamic weakening stage.

Hosted file

`image2.emf` available at https://authorea.com/users/560024/articles/608271-relationships-among-forearc-structure-fault-slip-and-earthquake-magnitude-numerical-simulations-with-

applications-to-the-central-chilean-margin

Figure S1. DEM model setup of the wedge profile.

Gravity is inclined 8° from the vertical axis, introducing a dipping basal surface. Blue and black layers serve as strain markers, but do not denote any change in properties.

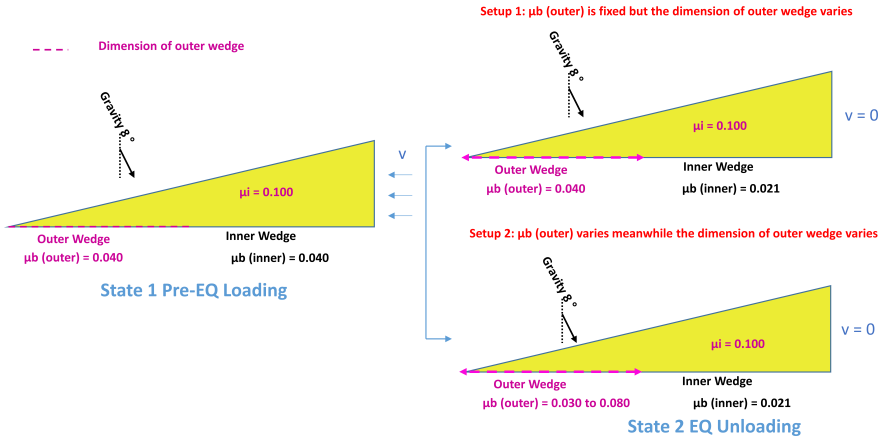

Figure S2. Simulation workflow (refer to Text S2 and Table S2).

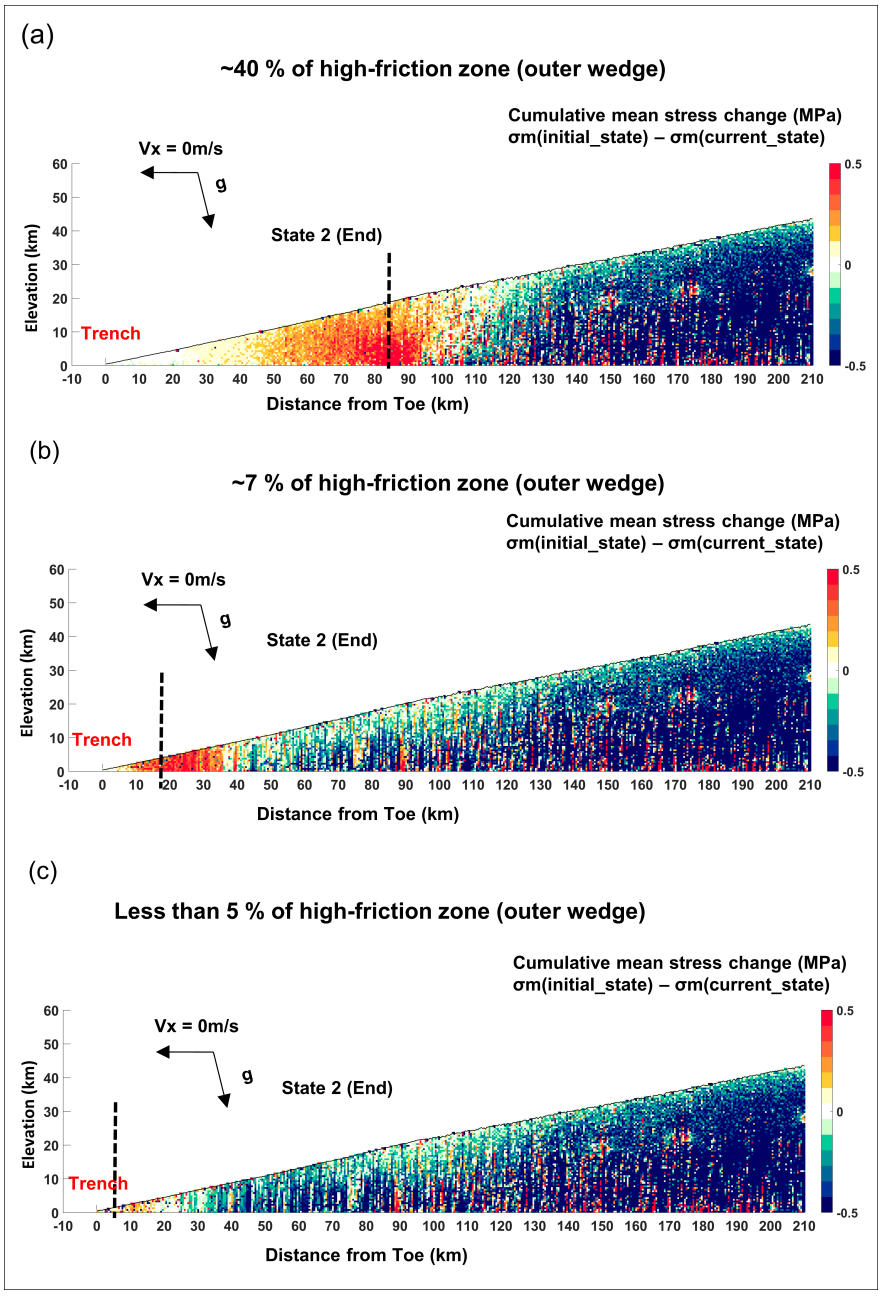

Figure S3. Simulated coseismic changes in mean stress to demonstrate stress transfer within the wedge for each earthquake.

(a) 2010 Maule earthquake, (b) 1960 Valdivia earthquake, and (c) 2011 Tohoku earthquake. Red indicates increase in mean stress blue indicates decrease. The black dashed line locates the boundary between the inner and outer wedges, marking a change in basal friction behavior.

Geophysical Research Letters

RESEARCH LETTER
10.1029/2021GL092521

Key Points:

- Upper plate structure and associated variations in megathrust frictional properties influence earthquake size and fault slip distributions
- Numerical simulations, validated by geophysical constraints, reproduce slip distributions for the 2010 Maule and 2011 Tohoku earthquakes
- The 1960 Valdivia earthquake likely experienced its highest slip close to the trench, in contrast to published models

Supporting Information:

Supporting Information may be found in the online version of this article.

Correspondence to:

X. Wang,
xw33@rice.edu

Citation:

Wang, X., Morgan, J. K., & Bangs, N. (2021). Relationships among forearc structure, fault slip, and earthquake magnitude: Numerical simulations with applications to the central Chilean margin. *Geophysical Research Letters*, *48*, e2021GL092521. https://doi.org/10.1029/2021GL092521

Received 13 JAN 2021
Accepted 8 JUN 2021

Relationships Among Forearc Structure, Fault Slip, and Earthquake Magnitude: Numerical Simulations With Applications to the Central Chilean Margin

Xiaoyu Wang[1], Julia K. Morgan[1], and Nathan Bangs[2]

[1]Department of Earth, Environmental and Planetary Sciences, Rice University, Houston, TX, USA, [2]Institute for Geophysics, University of Texas at Austin, Austin, TX, USA

Abstract Two adjacent segments of the Chile margin exhibit significant differences in earthquake magnitude and rupture extents during the 1960 Valdivia and 2010 Maule earthquakes. We use the discrete element method (DEM) to simulate the upper plate as having an inner and outer wedge defined by different frictional domains along the décollement. We find that outer wedge width strongly influences coseismic slip distributions. We use the published peak slip magnitudes to pick best fit slip distributions and compare our models to geophysical constraints on outer wedge widths for the margins. We obtain reasonable fits to published slip distributions for the 2010 Maule rupture. Our best-fit slip distribution for the 1960 Valdivia earthquake suggests that peak slip occurred close to the trench, differing from published models but being supported by new seismic interpretations along this margin. Finally, we also demonstrate that frictional conditions beneath the outer wedge can affect the coseismic slip distributions.

Plain Language Summary The south-central Chilean margin is host to the Mw 9.5 1960 Valdivia earthquake and the Mw 8.8 2010 Maule earthquake. Although their earthquake rupture segments are adjacent and partially overlap, the resulting earthquakes are significantly different. We use the DEM to explore the controls on these differences. We use assemblages of discrete particles to simulate wedges that define the upper plate in two dimensions. Each wedge is partitioned into a strong inner wedge, capable of supporting large elastic strains that can be released during earthquakes, and a lower strength outer wedge that resists earthquake rupture. We simulate earthquake unloading by instantaneously reducing the basal friction beneath the inner wedge for a range of relative widths of the outer wedge. The results yield a suite of slip distributions that can be compared with natural earthquake ruptures, including the Chilean events as well as the 2011 Tohoku earthquake. The best-fit slip distributions also provide constraints on the internal structure of the upper plate, which compares well to the interpreted structures in all three settings. Our simulations lead us to conclude that the 1960 Valdivia earthquake ruptured to the toe of the wedge, which differs from some previous interpretations.

1. Introduction

The south-central Chilean subduction margin is host to some of the largest megathrust earthquakes on Earth, including the greatest earthquake ever recorded on global networks, the Mw 9.5 1960 Valdivia earthquake. The largest earthquake along the margin since then was the Mw 8.8 2010 Maule earthquake, which partially overlaps and extends farther north from the Valdivia rupture (Figure 1a). Despite the proximity of the two source areas, the earthquake magnitudes, rupture extents, and efficiency of generating transoceanic tsunamis differ significantly between the 1960 and 2010 events. The 1960 Valdivia event ruptured a length of ~1,000 km of the Nazca-South America plate boundary along strike from 37°S to 46°S (Figure 1a). The subsequent trans-Pacific tsunami was so large that waves up to 25 m high reached the coast of Chile (Contreras-Reyes et al., 2010; M. S. Moreno et al., 2009). By comparison, the 2010 Maule earthquake ruptured a length of ~600 km from 33°S to 39°S (Figure 1a), producing a much smaller tsunami with average wave heights of 10 m (Contreras-Reyes et al., 2010; M. Moreno et al., 2010). The maximum coseismic slip accompanying the 2010 Maule earthquake was estimated to be ~20 m (M. Moreno et al., 2010; Tong et al., 2010), and fault slip models suggest that the rupture likely did not extend all the way to the trench, or if it did, the slip magnitude was very small (Delouis et al., 2010; Maksymowicz et al., 2017; M. Moreno et al., 2010, 2012; Tong et al., 2010). By comparison, the maximum coseismic slip during the 1960 Valdivia earthquake

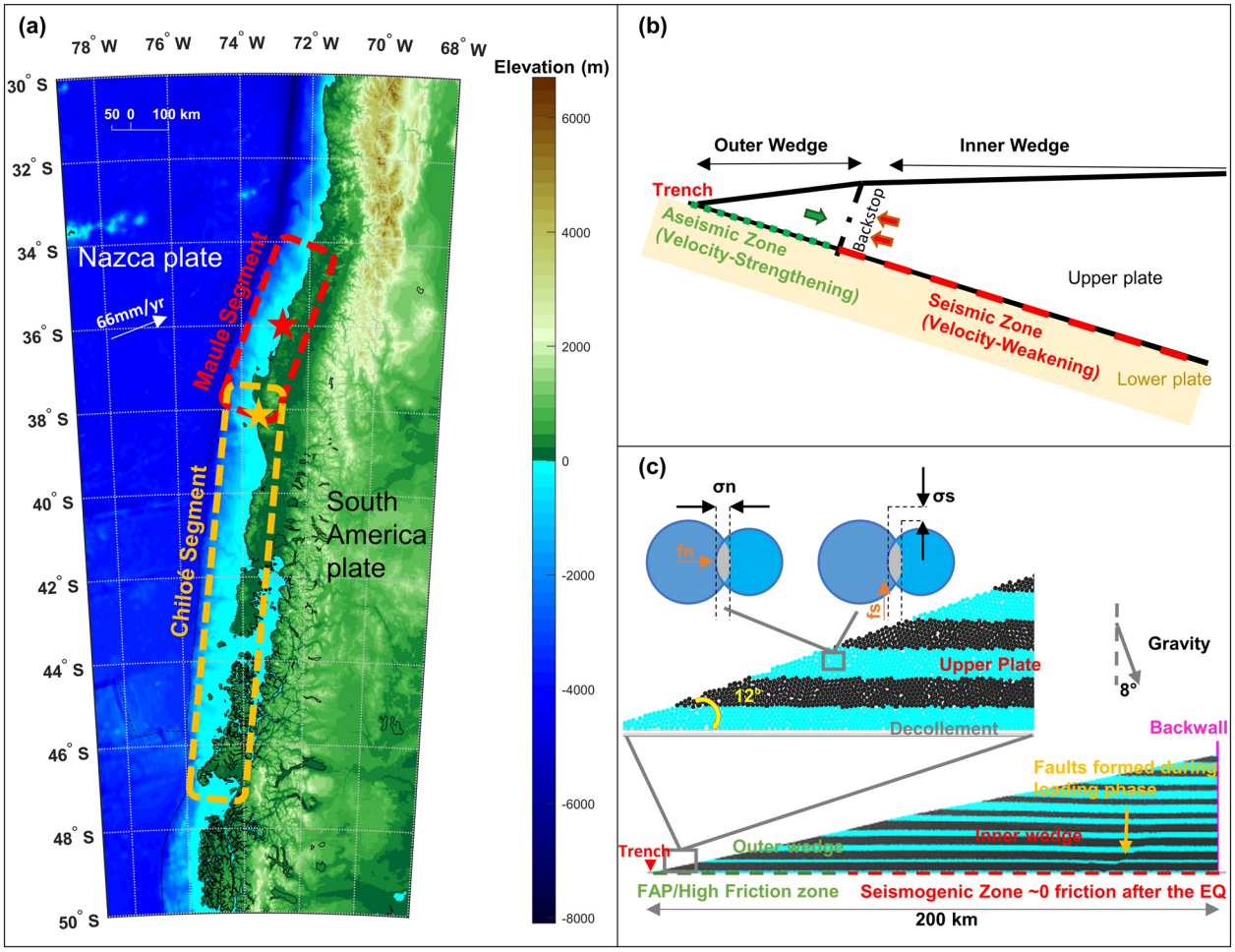

Figure 1. (a) The location map of the south-central Chile margin, showing the approximate 1960 Valdivia earthquake rupture area (yellow polygon) and the 2010 Maule earthquake rupture area (red polygon). (b) Conceptual model for the overriding continental plate consisting of an outer wedge (nominally aseismic zone, green dashed line) and inner wedge (seismic, velocity-weakening zone, red dashed line). (c) DEM model setup of the wedge profile; note that gravity is inclined, introducing a dipping basal surface.

exceeded ~40 m (M. S. Moreno et al., 2009). The peak displacement for the Valdivia event has been modeled ~100 km landward of the trench (M. S. Moreno et al., 2009), although this earthquake also is interpreted to have ruptured all the way to the trench (Barrientos & Ward, 1990; M. S. Moreno et al., 2009). The determinations for the coseismic slip distributions for the Valdivia earthquake, however, rely on sparsely sampled analog data, opening up the possibility that the modeled distributions are imprecise.

At subduction zones, the maximum slip magnitude during an earthquake is one potential measure of earthquake size. For a given margin, that magnitude likely depends on the extent of the megathrust fault that ruptures, defined by the updip limit of the seismogenic zone (Contreras-Reyes et al., 2010; Wang & Hu, 2006). Seaward of this limit, the fault is assumed to slip largely aseismically (Moore & Saffer, 2001; Scholz, 1998). Thus, the megathrust fault can be partitioned into an inner seismic or velocity-weakening zone, and an outer aseismic or velocity-strengthening zone. The contrasting frictional behavior of these two zones also influences the upper plate geometry and deformation, partitioning the upper plate into corresponding inner and outer wedges (Wang & Hu, 2006), as shown in Figure 1b. The more deformable outer wedge, composed of relatively young unconsolidated sediments, is presumed to resist coseismic slip and undergo internal deformation during an earthquake. The inner wedge, consisting of older well-lithified accreted sediments and basement rocks, is more prone to fault locking during the interseismic period, and rapid slip during earthquake ruptures (Wang & Hu, 2006). Along the south-central Chilean margin, the boundary between the inner and outer wedge has been defined by the location of a geophysically constrained

backstop (Contreras-Reyes et al., 2010). Thus, upper plate structure can provide another tool for evaluating the seismic potential of a subduction margin. In fact, Contreras-Reyes et al. (2010) interpreted that the width of the outer wedge in the 1960 rupture area is smaller than the one in the 2010 rupture area (Table S1, Supporting Information), suggesting an inverse relationship between outer wedge width and earthquake size (Contreras-Reyes et al., 2010, 2017; Wang & He, 2008). This hypothesis, however, is based on limited data and uncertain interpretations of both wedge width and earthquake slip distributions (Langer, 2020).

Building on recent modeling efforts investigating the controls on extensional deformation in the Japan Trench forearc following the Tohoku earthquake (Wang & Morgan, 2019), we use numerical simulations to estimate the megathrust slip distributions that would arise from different ratios of inner and outer wedges for a reference subduction zone, and then compare the magnitudes of megathrust slip to published slip distributions for the Valdivia and Maule earthquakes. The well-documented Tohoku earthquake also provides a valuable point of comparison, as it also experienced trench breaking rupture (Ito et al., 2011; Sun et al., 2017; Wang & Tréhu, 2016) and thus is a useful analog for the less well-constrained Valdivia event. The selected best-fit simulated slip distributions for the Maule and Tohoku earthquakes prove to be consistent with geophysical interpretations for transitions between the inner to outer wedges along each margin. In contrast, the landward position of the peak slip zone interpreted for the Valdivia event (M. S. Moreno et al., 2009) conflicts with the small interpreted outer wedge along the margin and the large coseismic peak slip. We suggest that our simulated coseismic slip model represents a more realistic distribution for this great earthquake.

2. Approach and Methodology

RICEBAL, a discrete element method (DEM) based program, is used to construct the models used here. Details about the DEM methodology can be found in the supplementary materials, as well as previous publications (Morgan, 2015; Wang & Morgan, 2019). The particle sizes and their mechanical properties are tabulated in the supplementary materials (S1).

The initial wedge is constructed by randomly generating particles within a two-dimensional 200 km wide domain and letting them settle under gravity. The settled particles are then sculpted to the desired wedge shape with a starting taper angle of 12° ($\alpha + \beta$), based on published geometries for the SC Chile margin (Maksymowicz, 2015), and subjected to gravity tilted at an angle of 8° from the vertical, simulating a fixed megathrust dip angle (β) of 8°. The initial full length of the wedge is 200 km, comparable to the down-dip rupture distance along the central Chile margin (Figure 1a). Following particle deposition and wedge sculpting, bonds are added between particles in contact within the wedge to impart cohesion.

The wedge is divided into inner and outer wedge domains, distinguished by the assigned values of basal friction on the underlying megathrust fault (Figure 1c). The mechanical properties of the domains and interfaces are controlled by the particle properties and interparticle friction coefficients assigned for each domain. The derivation of the bulk internal friction (μ'_{int}) and basal friction (μ'_{bas}) of the inner and outer wedges, respectively (Table S2, Supporting Information), is explained in the supplementary materials and previous studies (Morgan, 2015; Wang & Morgan, 2019). We use a highly simplified model that focuses on the first-order effects of fault properties and outer wedge width on earthquake sizes during an earthquake cycle. Therefore, we employ constant values of basal friction across each of the inner or outer wedges for a given simulation stage, ignoring the spatial and temporal variations that likely occur in nature.

Each numerical simulation is carried out in two stages: Stage 1) pre-earthquake loading under "static" basal friction values, and Stage 2) dynamic release of the stored strain energy under reduced basal friction beneath the inner wedge, which corresponds to earthquake rupture. This decrease in friction is a simplified way to simulate velocity-weakening, thought to accompany great earthquakes within the subduction seismogenic zones, theoretically causing rupture propagation or even extensional failure (Wang & Hu, 2006; Wang & Morgan, 2019). During the first stage, the backwall is displaced at a steady rate, while the slip of the wedge is resisted by basal friction. This causes the build-up of elastic strain energy within the wedge and increases shear stresses along the megathrust. Stage 1 terminates after 8 km of backwall displacement, when the fault is preconditioned and poised for failure. The length of the wedge decreases during the preconditioning stage

as it accumulates elastic strain. Earthquake rupture is induced during Stage 2 by instantaneously decreasing the basal friction beneath the inner wedge, which results in dynamic slip along the underlying fault. Concurrently, the basal friction beneath the outer wedge is either maintained or increased, simulating a more resistant outer wedge. More information about the modeling workflow can be found in the supplementary materials (S2) and the previous work (Wang & Morgan, 2019).

We carried out two different simulation setups, each one using different combinations of basal friction and friction changes for a range of different outer wedge widths, as shown in Table S2 (Supporting Information). In all models, the internal friction coefficient (μ'_{int}) was maintained at 0.100 for both the inner and outer wedges.

Our first model setup (Table S2, Supporting Information) was designed to determine how the width of the outer wedge (velocity strengthening zone) affects the distribution of fault slip during earthquake rupture. Based on our simulation trials and previous studies on constraining the effective strength of the megathrust and forearc in the Maule area (Dielforder, 2017; Wang & Hu, 2006), the effective basal friction coefficients for the inner and outer wedges, $\mu'_{\text{bas\_inner}}$ and $\mu'_{\text{bas\_outer}}$, respectively, were both set to 0.040 at the start of the pre-earthquake loading stage. During the earthquake rupture phase, $\mu'_{\text{bas\_inner}}$ was instantly decreased to 0.021 while $\mu'_{\text{bas\_outer}}$ was maintained at 0.040. Simulations were conducted for a range of outer wedge widths.

The second model setup (Table S2, supporting information) was used to investigate the effects of the coefficient of friction and friction change beneath the outer wedge during earthquake rupture, on slip magnitude and distribution. As above, the effective basal friction values for both the inner and outer wedges, $\mu'_{\text{bas\_inner}}$ and $\mu'_{\text{bas\_outer}}$ respectively, were initially assigned to 0.040 during the pre-earthquake loading stage. Then during the earthquake rupture phase, $\mu'_{\text{bas\_inner}}$ was instantly decreased to 0.021 to simulate velocity weakening. Concurrently $\mu'_{\text{bas\_outer}}$ also was changed to different values, ranging from 0.040 to 0.080.

3. Simulation Results

The instantaneous reduction in basal friction beneath the inner wedge allowed the simulated wedge to slip along the fixed lower plate as it unloaded, interacting with the outer wedge, which also had the potential to slip and unload. The final coseismic slip distributions for both inner and outer wedges were calculated by tracking average particle displacements within 2,000 × 1,000 m domains immediately above the fault zone. For presentation purpose, the trench and wedge toe are placed at 0 km.

For Setup 1, 17 simulations were conducted using different ratios of outer wedge length to full wedge length, ranging from 0% to ~60% of the full wedge length; the final displacements, from the wedge toe (at 0 km) to the backwall, at the end of unloading are summarized in Figures 2a–2b (Note, the small step in displacement that occurs at ~170 km on all curves is due to reactivation of a fault that formed during preconditioning, as explained in the supplementary material.) This fault does not contribute significantly to the coseismic rupture distribution). Several clear patterns emerge from this plot: the fault displacement generally increases from the backwall to the toe, until it is suppressed by the resistant outer wedge. Thus, the magnitude of peak coseismic slip and the distance to the peak correlate inversely with the width of the outer wedge (Figure 2a). These relationships can provide very useful constraints on wedge structure. In particular, large peak slip occurs very close to the toe if the outer wedge is very small, i.e., less than 10% of the megathrust fault length (Figure 2a) but decreases in magnitude and shifts away from the toe as the outer wedge width increases. As the slip magnitude decreases noticeably near the transition from the inner to the outer wedge, the peak slip magnitude increases exponentially as the width of the outer wedge decreases (Figure 2b). In our simulations, some coseismic rupture propagates to the trench in all cases, although decreasing with increasing outer wedge width. We attribute this tendency to the uniform internal friction across both the inner and outer wedges, which prevents the outer wedge from accumulating significant internal deformation. This is likely not true for most natural systems.

Interestingly, all simulations undergo identical preconditioning stages, thus each wedge stores the same amount of elastic strain energy prior to earthquake unloading. The amount of energy released during the

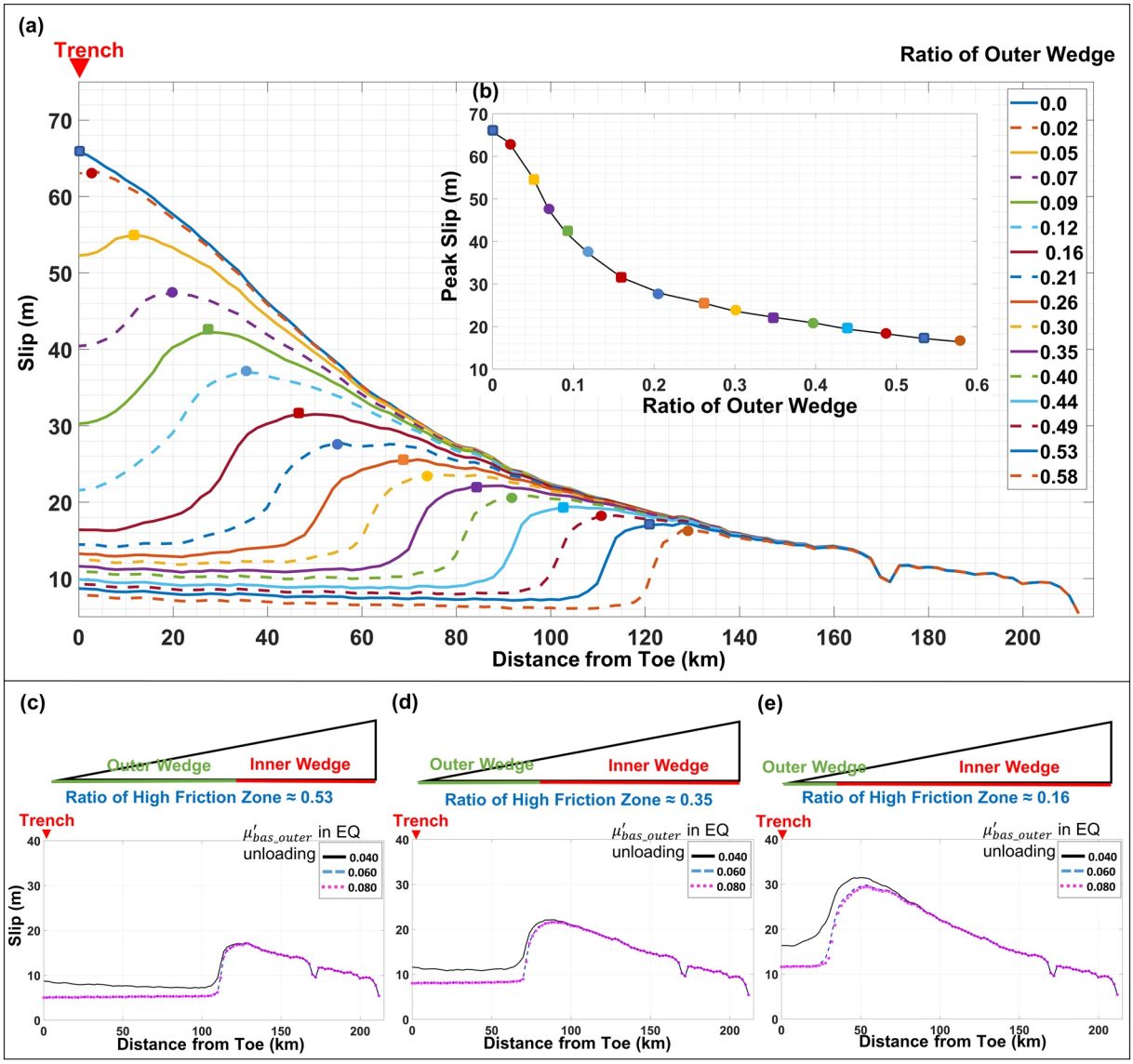

Figure 2. (a) Coseismic slip distributions along the décollement for different ratios of the outer wedge. (b) Peak slip values from the coseismic slip distributions versus outer wedge ratio. Coseismic slip distributions along the décollement for different changes in basal friction beneath the outer wedge for outer wedge ratios of (c) 0.53 (d) 0.35, and (e) 0.16.

simulated earthquakes, however, differs for each model. This is reflected by the position and magnitude of the peak slip, which is controlled primarily by the width of the outer wedge. Thus, for the reference subduction system simulated here, we can use the position and value of peak slip as a measure of earthquake size.

With Setup 2, we compared three different outer wedge widths, and examined the effects of four different changes in friction beneath the outer wedge (Figures 2c–2e). We see that the friction magnitude primarily influences the coseismic slip magnitude beneath the outer wedge, and only secondarily, the peak slip magnitude, specifically for the smallest wedge ratios (Figure 2e). As seen in Figure 2a, all models exhibit a step-in slip magnitude near the boundary between the inner and outer wedges; however, the larger the reduction in outer wedge friction, the greater the cumulative fault slip. For $\mu'_{\mathrm{bas\_outer}}$ larger than 0.040 (i.e., velocity strengthening), the coseismic slip distributions beneath the outer wedge are similar and small (blue dashes and pink circles in Figures 2c–2e). In the case of constant friction ($\mu'_{\mathrm{bas\_outer}} = 0.040$, black line), the

outer wedge experiences higher fault slip. As above, the step-in displacement at ~170 km is due to a pre-existing fault.

4. Discussion

4.1. Controls on Earthquake Magnitudes and Coseismic Slips

Our simulations demonstrate that the heterogeneity of basal friction has an impact on rupture extents and slip magnitudes, and to first-order, the magnitude of peak fault slip has an inverse relationship with outer wedge size. Based on published values of peak slip for earthquakes along the south-central Chile margin, we can select results from our Setup 1 simulations (Figure 2a) that yield maximum fault slip magnitudes that reasonably match the peak slip values for 2010 Maule earthquakes and 1960 Valdivia earthquakes. Figure 3 shows ranges of simulation results (black and gray lines) that best fit the published slip distributions for those two events (shaded bands). The peak slip magnitude and position derived for the Maule earthquake is well fit by models with an outer wedge of ~40% of the subduction interface (Figure 3a). However, to match the peak slip magnitude for the Valdivia earthquake, we must select results for smaller outer wedges, i.e., ~7% of the subduction interface (Figure 3b), which shift the peaks significantly seaward than modeled previously (M. S. Moreno et al., 2009). We also present best-fit simulated slip distributions that reasonably match the preferred slip range of Sun et al. (2017) for the well-instrumented 2011 Tohoku earthquake offshore Japan (Figure 3c). Our simulations require a very small outer wedge of ~5%, similar to the Valdivia case. The Tohoku earthquake is known to have ruptured all the way to the trench (Ito et al., 2011; Sun et al., 2017; Wang & Tréhu, 2016), and thus serves as a good analog for the Valdivia earthquake (Note, the corresponding model-derived stress changes for the simulated earthquakes can be found in the supplementary materials S3.)

The inverse relationship between the ratio of the outer wedge and the magnitude of peak fault slip (Figure 2a) yield predictions for widths of outer wedges that can be compared with constraints for upper plate structure along the margins that hosted each of these earthquakes.

Tomographic models for the 2010 Mw 8.8 Maule earthquake rupture segment (Contreras-Reyes et al., 2010, 2017) suggest a relatively large outer wedge zone consistent with the interpreted peak slip of about 20 m (Table S1, Supporting Information). Our best-fit slip distribution corresponds to an outer wedge ~40% of the subduction interface and an outer wedge friction value of 0.040 (Figure 3a). Our simulated peak slip is about 22 m, located ~80 km from the trench, which is broadly consistent with the derived slip distribution (blue dashed curve) for the 2010 Maule earthquake (M. Moreno et al., 2012).

The Valdivia rupture segment is thought to have a smaller outer wedge than the Maule segment, based on recent seismic interpretations (Bangs et al., 2020). The simulation with a ~15 km wide outer wedge (over 7% of the subduction interface) provides a reasonable fit to the peak coseismic slip of ~44 m (Figure 3b, left panel). However, to obtain such large simulated slip in our models, coseismic rupture must have extended all the way to the trench, which differs from the published peak slip, which occurs ~100 km from the trench (M. S. Moreno et al., 2009). These derived slip values are consistent with previous studies that suggested the highest slip of the 1960 earthquake was over twice the peak slip triggered by the 2010 earthquake, and that the earthquake ruptured all the way to the trench (Contreras-Reyes et al., 2010; M. S. Moreno et al., 2009). Thus, we interpret that the highest slip patch for the 1960 earthquake was much closer to the trench than previously modeled (M. S. Moreno et al., 2009).

The 2011 Mw 9.0 Tohoku earthquake and the simulated coseismic slip distribution compare well to the 1960 Valdivia earthquake. Previous studies (Ide et al., 2011; Wang & Tréhu, 2016) proposed that a coseismic drop in friction beneath a small outer wedge along the Tohoku margin contributed to the large displacement and dynamic overshoot during the Tohoku earthquake. Thus, the Tohoku earthquake is a good analog to the Valdivia earthquake, which also is interpreted to have a small outer wedge. We interpret that significant dynamic weakening during the Valdivia earthquake also overwhelmed the very small zone where dynamic strengthening occurred (e.g., Wang & Hu, 2006). The Tohoku earthquake ruptured all the way to the trench (Ide et al., 2011; Ito et al., 2011; Tsuji et al., 2011), and the highest coseismic slip was ~64 m very close to the trench (Sun et al., 2017; Tsuji et al., 2011; Wei et al., 2012). This slip distribution is consistent with our

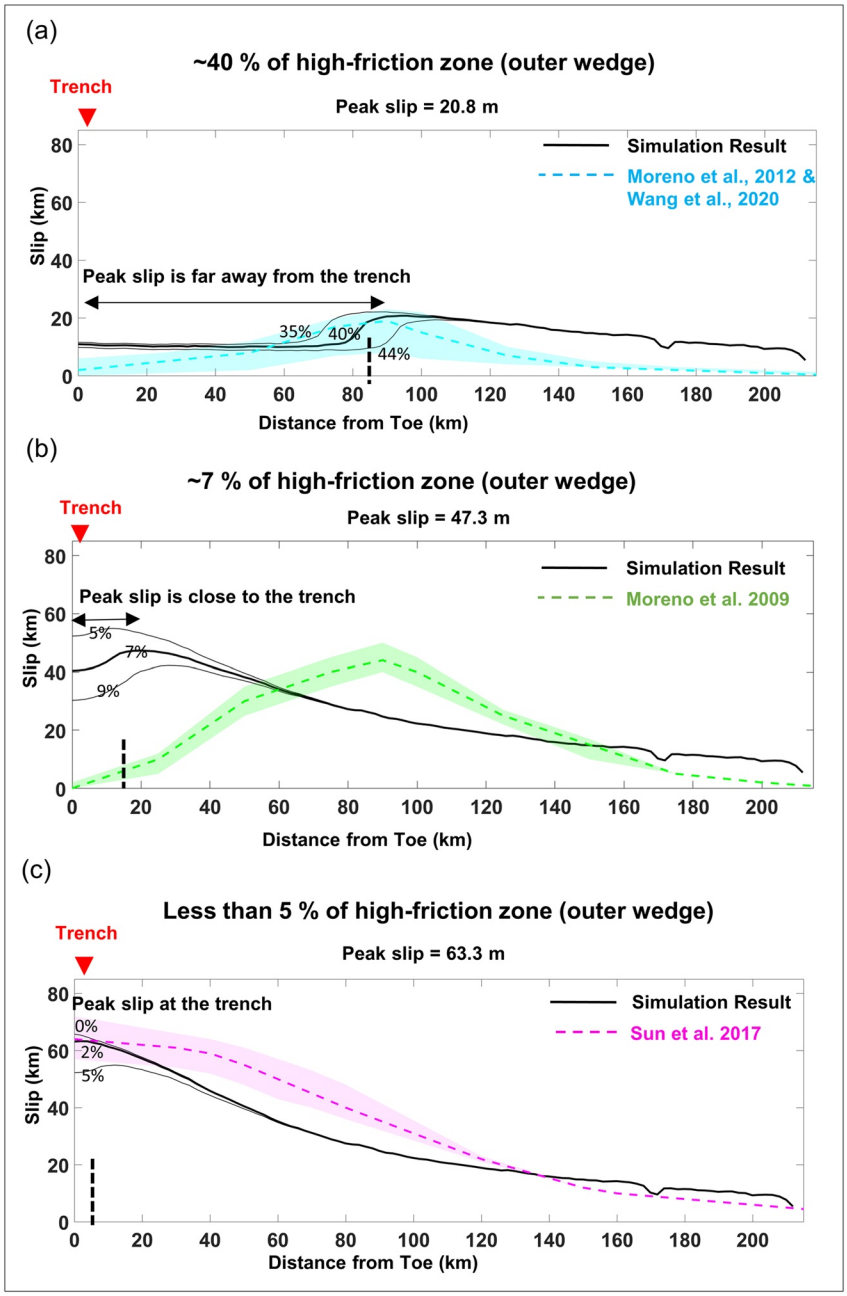

Figure 3. Simulated coseismic slip scenarios compared with derived slip models. (a) 2010 Maule earthquake rupture (Moreno et al., 2012), blue shading indicates the range of slip models from (Wang et al., 2020). (b) 1960 Valdivia earthquake rupture (Moreno et al., 2009), green shading indicates the range in slip distributions across the two peak slip patches from the models of Moreno et al. (2009). (c) 2011 Tohoku earthquake rupture, pink shading captures the preferred model range (Sun et al., 2017).

results for a very small outer wedge, i.e., less than 5% of the full wedge width (Figure 3c), leading to peak slip very close to the trench. In this case, the small outer wedge offered little resistance to slip, allowing significant stress decrease throughout the wedge (Figure S3c). Similar to the Tohoku event, the Valdivia earthquake also produced an enormous tsunami, which strongly suggests significant displacement of the toe. The new geophysical constraints on the small width of the outer wedge along this margin (Bangs et al., 2020) provide corroborating support for trench-breaking rupture.

Our numerical simulations used an idealized distribution of friction along the modeled megathrust fault, which has a sharp updip transition at the inner and outer wedge boundary. This results in the relatively sharp drops in fault slip near the inner and outer wedge boundaries. In addition, the downdip boundary of the frictional megathrust is sharply defined by the position of the backwall. These simplified boundary conditions can result in slip distributions that differ from the natural system. For example, in nature, friction across the inner to outer wedge transition is likely much more gradational, which would result in more gradual decreases in slip toward the toe as documented for the Maule event (M. Moreno et al., 2012). Velocity strengthening in the downdip region that we do not model here, might shift the position of the peak slip away from the inner to outer wedge transition (Wang & He, 2008). Despite these approximations, the coseismic slip distributions derived for our simplified models generally agrees with interpretations for the widths of the outer wedges in all three locations, as well as the peak slip values. Our results, however, invite reconsideration of the location of the peak slip for the Valdivia earthquake shifting it significantly seaward. Finally, our simulations demonstrate that upper plate structure can provide good first-order constraints on earthquake slip distributions in all settings.

4.2. Effects of Velocity Strengthening on Coseismic Ruptures

Our results from Setup 2 provide further insights into how spatial and temporal variations in fault strength during earthquakes can influence earthquake rupture behavior. Figures 2c–2e demonstrate how coseismic changes in outer wedge friction affect the slip distribution and magnitude. If the outer wedge experiences coseismic strengthening (i.e., basal friction increases from 0.040 to 0.060–0.080) as inferred in Wang and Hu (2006) model, this results in a ∼25% reduction in the magnitude of outer wedge slip, reflecting the increased fault resistance. The peak slip magnitude is also slightly reduced, most noticeably for the smallest outer wedge (Figure 2e).

The trends revealed by all these simulations demonstrate that both width and frictional properties of an outer wedge will play a significant role in how slip is distributed across a megathrust fault during an earthquake, and whether the rupture can extend all the way to the toe, where it might generate a large tsunami. A large outer wedge that is frictionally strong resists seaward slip and absorbs much of the stress released from the inner wedge during an earthquake, limiting displacement at the wedge toe.

5. Conclusions

Our simulations demonstrate that both the width and frictional properties of the outer wedge affects slip distribution and magnitude along active subduction margins. Our simulated slip distributions yield important insights into the wedge properties and frictional changes that accompanied the 2010 Maule earthquake and the 1960 Valdivia earthquake rupture, along the central Chilean margin, as well as for the 2011 Tohoku earthquake off Japan. Constrained by published peak slip values for these earthquakes along with plausible values of megathrust friction during pre-earthquake loading and coseismic earthquake rupture (Dielforder, 2017; Wang & Hu, 2006), our simulations yield predicted slip distributions for the three events. Our results also show consistency with published geophysical constraints on the locations and widths of the outer wedge. Importantly, combining our best-fit simulation results for the peak slip magnitude for the 1960 Valdivia earthquake, and new geophysical interpretation for a narrow outer wedge along this margin, allows us to argue for a refined coseismic slip distribution for the Valdivia event, in which the maximum slip of ∼44 m occurred closer to the toe than what is inferred from slip models derived from earthquake records (M. S. Moreno et al., 2009). This conclusion is consistent with evidence for the maximum slip at the toe for another recent megathrust rupture, the well-instrumented Tohoku earthquake (Ide et al., 2011; Sun et al., 2017).

The parameter study carried out using Setup 1 (Figures 2a–2b) suggests that seismic hazards can be characterized more easily when we know the forearc structure. Thus, the interpretation of forearc structure bundled with corresponding numerical simulations can predict coseismic slip distributions for poorly instrumented earthquakes. Moreover, the numerical simulations, calibrated to match available slip distributions and the estimated widths of the frontal wedge, can be used to run parameter tests to create a template showing the correlation among the width of the outer wedge, coseismic rupture, and the slip distributions

for various coseismic friction changes. This template could allow us to quickly assess the coseismic slip displacement and amplitude of the rupture for different localities lacking records of megathrust earthquakes, assuming the geometry of the frontal wedge can be estimated.

We also show that slip distributions and peak slip magnitudes of ruptures are sensitive to frictional changes during earthquakes (Figures 2c–2e). The outer wedge frictional behavior can play a significant role in controlling fault displacement distribution and peak slip when the width of the outer wedge is sufficiently small, such as along the Valdivia rupture segment. Combining estimates of the widths and basal frictional changes of the outer wedges, therefore, can help us better predict the future sizes of the earthquakes and their associated risks.

Data Availability Statement

The modeling results, corresponding files, raw data, and sample code for this research can be found in the published data set https://doi.org/10.6084/m9.figshare.13565447.v1.

Acknowledgments
This work was funded in part by National Science Foundation grant EAR-1723249. Computing facilities were made available in part through the Rice Center for Computational Geophysics. The authors also would like to thank Dr. Armin Dielforder and another anonymous reviewer for the helpful comments on earlier drafts of the manuscript. Interested parties are encouraged to contact the author to request copies of animated GIFs of the simulations for further study.

References

Bangs, N., Morgan, J., Tréhu, A., Contreras-Reyes, E., Arnulf, A., Han, S., et al. (2020). Basal accretion along the south central Chilean margin and its relationship to great earthquakes. *Journal of Geophysical Research: Solid Earth*, *125*(11), e2020JB019861. https://doi.org/10.1029/2020jb019861

Barrientos, S. E., & Ward, S. N. (1990). The 1960 Chile earthquake: Inversion for slip distribution from surface deformation. *Geophysical Journal International*, *103*(3), 589–598. https://doi.org/10.1111/j.1365-246x.1990.tb05673.x

Contreras-Reyes, E., Flueh, E. R., & Grevemeyer, I. (2010). Tectonic control on sediment accretion and subduction off south central Chile: Implications for coseismic rupture processes of the 1960 and 2010 megathrust earthquakes. *Tectonics*, *29*(6).

Contreras-Reyes, E., Maksymowicz, A., Lange, D., Grevemeyer, I., Muñoz-Linford, P., & Moscoso, E. (2017). On the relationship between structure, morphology and large coseismic slip: A case study of the Mw 8.8 Maule, Chile 2010 earthquake. *Earth and Planetary Science Letters*, *478*, 27–39. https://doi.org/10.1016/j.epsl.2017.08.028

Delouis, B., Nocquet, J. M., & Vallée, M. (2010). Slip distribution of the February 27, 2010 Mw = 8.8 Maule earthquake, central Chile, from static and high-rate GPS, InSAR, and broadband teleseismic data. *Geophysical Research Letters*, *37*(17). https://doi.org/10.1029/2010gl043899

Dielforder, A. (2017). Constraining the strength of megathrusts from fault geometries and application to the Alpine collision zone. *Earth and Planetary Science Letters*, *474*, 49–58. https://doi.org/10.1016/j.epsl.2017.06.021

Ide, S., Baltay, A., & Beroza, G. C. (2011). Shallow dynamic overshoot and energetic deep rupture in the 2011 Mw 9.0 Tohoku-oki earthquake. *Science*, *332*(6036), 1426–1429. https://doi.org/10.1126/science.1207020

Ito, Y., Tsuji, T., Osada, Y., Kido, M., Inazu, D., Hayashi, Y., et al. (2011). Frontal wedge deformation near the source region of the 2011 Tohoku-oki earthquake. *Geophysical Research Letters*, *38*(7). https://doi.org/10.1029/2011gl048355

Langer, L. (2020). *Impact of topography on coseismic modeling and earthquake static slip inversions*. Princeton University.

Maksymowicz, A. (2015). The geometry of the Chilean continental wedge: Tectonic segmentation of subduction processes off Chile. *Tectonophysics*, *659*, 183–196. https://doi.org/10.1016/j.tecto.2015.08.007

Maksymowicz, A., Chadwell, C., Ruiz, J., Tréhu, A., Contreras-Reyes, E., Weinrebe, W., et al. (2017). Coseismic seafloor deformation in the trench region during the Mw8. 8 Maule megathrust earthquake. *Scientific Reports*, *7*(1), 1–8. https://doi.org/10.1038/srep45918

Moore, J. C., & Saffer, D. (2001). Updip limit of the seismogenic zone beneath the accretionary prism of southwest Japan: An effect of diagenetic to low-grade metamorphic processes and increasing effective stress. *Geology*, *29*(2), 183–186. https://doi.org/10.1130/0091-7613(2001)029<0183:ulotsz>2.0.co;2

Moreno, M., Melnick, D., Rosenau, M., Baez, J., Klotz, J., Oncken, O., et al. (2012). Toward understanding tectonic control on the Mw 8.8 2010 Maule Chile earthquake. *Earth and Planetary Science Letters*, *321*, 152–165. https://doi.org/10.1016/j.epsl.2012.01.006

Moreno, M., Rosenau, M., & Oncken, O. (2010). Maule earthquake slip correlates with pre-seismic locking of Andean subduction zone. *Nature*, *467*(7312), 198–202. https://doi.org/10.1038/nature09349.2010

Moreno, M. S., Bolte, J., Klotz, J., & Melnick, D. (2009). Impact of megathrust geometry on inversion of coseismic slip from geodetic data: Application to the 1960 Chile earthquake. *Geophysical Research Letters*, *36*(16). https://doi.org/10.1029/2009gl039276

Morgan, J. K. (2015). Effects of cohesion on the structural and mechanical evolution of fold and thrust belts and contractional wedges: Discrete element simulations. *Journal of Geophysical Research: Solid Earth*, *120*(5), 3870–3896. https://doi.org/10.1002/2014jb011455

Scholz, C. H. (1998). Earthquakes and friction laws. *Nature*, *391*(6662), 37–42. https://doi.org/10.1038/34097

Sun, T., Wang, K., Fujiwara, T., Kodaira, S., & He, J. (2017). Large fault slip peaking at trench in the 2011 Tohoku-oki earthquake. *Nature Communications*, *8*(1), 1–8. https://doi.org/10.1038/ncomms14044

Tong, X., Sandwell, D., Luttrell, K., Brooks, B., Bevis, M., Shimada, M., et al. (2010). The 2010 Maule, Chile earthquake: Downdip rupture limit revealed by space geodesy. *Geophysical Research Letters*, *37*(24). https://doi.org/10.1029/2010gl045805

Tsuji, T., Ito, Y., Kido, M., Osada, Y., Fujimoto, H., Ashi, J., et al. (2011). Potential tsunamigenic faults of the 2011 off the Pacific coast of Tohoku earthquake. *Earth, Planets and Space*, *63*(7), 58. https://doi.org/10.5047/eps.2011.05.028

Wang, K., & He, J. (2008). Effects of frictional behavior and geometry of subduction fault on coseismic seafloor deformation. *Bulletin of the Seismological Society of America*, *98*(2), 571–579. https://doi.org/10.1785/0120070097

Wang, K., & Hu, Y. (2006). Accretionary prisms in subduction earthquake cycles: The theory of dynamic Coulomb wedge. *Journal of Geophysical Research: Solid Earth*, *111*(B6). https://doi.org/10.1029/2005jb004094

Wang, K., Huang, T., Tilmann, F., Peacock, S. M., & Lange, D. (2020). Role of serpentinized mantle wedge in affecting megathrust seismogenic behavior in the area of the 2010 M = 8.8 Maule earthquake. *Geophysical Research Letters*, *47*(22), e2020GL090482. https://doi.org/10.1029/2020gl090482

Wang, K., & Tréhu, A. M. (2016). Invited review paper: Some outstanding issues in the study of great megathrust earthquakes—The Cascadia example. *Journal of Geodynamics*, *98*, 1–18. https://doi.org/10.1016/j.jog.2016.03.010

Wang, X., & Morgan, J. K. (2019). Controls on fore-arc deformation and stress switching after the great 2011 Tohoku-Oki earthquake from discrete numerical simulations. *Journal of Geophysical Research: Solid Earth*, *124*(8), 9265–9279. https://doi.org/10.1029/2019jb017420

Wei, S., Graves, R., Helmberger, D., Avouac, J.-P., & Jiang, J. (2012). Sources of shaking and flooding during the Tohoku-oki earthquake: A mixture of rupture styles. *Earth and Planetary Science Letters*, *333*, 91–100. https://doi.org/10.1016/j.epsl.2012.04.006

References From the Supporting Information

Guo, Y., & Morgan, J. K. (2004). Influence of normal stress and grain shape on granular friction: Results of discrete element simulations. *Journal of Geophysical Research: Solid Earth*, *109*(B12). https://doi.org/10.1029/2004jb003044

Guo, Y., & Morgan, J. K. (2006). The frictional and micromechanical effects of grain comminution in fault gouge from distinct element simulations. *Journal of Geophysical Research: Solid Earth*, *111*(B12). https://doi.org/10.1029/2005jb004049

Morgan, J. K., & Boettcher, M. S. (1999). Numerical simulations of granular shear zones using the distinct element method: 1. Shear zone kinematics and the micromechanics of localization. *Journal of Geophysical Research: Solid Earth*, *104*(B2), 2703–2719. https://doi.org/10.1029/1998jb900056

Morgan, J. K., & McGovern, P. J. (2005a). Discrete element simulations of gravitational volcanic deformation: 1. Deformation structures and geometries. *Journal of Geophysical Research: Solid Earth*, *110*(B5). https://doi.org/10.1029/2004jb003252

Morgan, J. K., & McGovern, P. J. (2005b). Discrete element simulations of gravitational volcanic deformation: 2. Mechanical analysis. *Journal of Geophysical Research: Solid Earth*, *110*(B5). https://doi.org/10.1029/2004jb003253

Thornton, C., & Barnes, D. (1986). Computer simulated deformation of compact granular assemblies. *Acta Mechanica*, *64*(1–2), 45–61. https://doi.org/10.1007/bf01180097